Energy & Environmental Science

COMMUNICATION

View Article Online
View Journal | View Issue

Cite this: *Energy Environ. Sci.*, 2019, **12**, 945

Received 9th October 2018,
Accepted 31st January 2019

DOI: 10.1039/c8ee02981d

rsc.li/ees

Elucidating the mobility of H^+ and Li^+ ions in $(Li_{6.25-x}H_xAl_{0.25})La_3Zr_2O_{12}$ *via* correlative neutron and electron spectroscopy†‡

Xiaoming Liu, §[a] Yan Chen, §[b] Zachary D. Hood, [ac] Cheng Ma,[d] Seungho Yu, [e] Asma Sharafi,[e] Hui Wang,[f] Ke An, [b] Jeff Sakamoto,[e] Donald J. Siegel, [eg] Yongqiang Cheng,*[b] Niina H. Jalarvo *[bh] and Miaofang Chi *[a]

A major challenge toward realizing high-performance aqueous lithium batteries (ALBs) is the utilization of a metallic lithium anode. However, an ideal solid electrolyte that can protect metallic lithium from reacting with aqueous solutions while still maintaining a high lithium ion conduction is not currently available. One obstacle is the lack of a reliable experimental tool to differentiate the conduction behaviour of H^+ and Li^+ ions in a solid electrolyte. Here, by correlating neutron and electron spectroscopy, we quantitatively reveal the mobility and lattice occupancy of the two ions individually in protonated cubic $Li_{6.25}Al_{0.25}La_3Zr_2O_{12}$ (LLZO). Our results not only highlight LLZO as a potential effective separation layer for ALBs but also present a robust method to quantify the mobility of individual mobile ions in solid-state ion conductors.

Broader context

Aqueous lithium batteries (ALBs) represent one of the best candidates for large scale energy storage, in the realization of the full use of renewable energy sources. A major challenge toward achieving high-performance ALBs lies in the utilization of metallic lithium as the anode. An ideal solid electrolyte "enabler" that can protect metallic lithium from reacting with aqueous solutions while maintaining a high lithium ion conduction is not currently available. One obstacle is the lack of a reliable experimental tool to measure the conduction behaviour of H^+ and Li^+ ions in a solid electrolyte. Here, by correlating neutron and electron spectroscopy, we quantitatively reveal the mobility and lattice occupancy of the H^+ and Li^+ ions individually in protonated cubic $Li_{6.25}Al_{0.25}La_3Zr_2O_{12}$ (H-LLZO). Our results show that within the operation temperature range of ALBs, H^+ ions are immobile while Li^+ ions maintain a desired mobility even in H-LLZO with a high H^+ concentration. These results highlight LLZO as a potential effective separation layer for ALBs. More importantly, our work provides a new method to probe diffusion behavior of individual ion species in dual-ion solids, an important family of materials for energy storage, environmental sensing, neuromorphic computing, and beyond.

Increased environmental concerns have motivated the use of sustainable and renewable energy sources. However, efficient storage of this energy in large quantities and at low cost remains a challenge. Li-ion batteries (LIBs) are widely used in portable electronics due to their relatively high energy densities compared to competing battery chemistries.[1–6] Despite these successes, batteries with increased energy and power densities are desirable for applications in powering electric vehicles and for grid energy storage.[1,3,7–10] Thus, there is a clear need for new and advanced battery configurations.

[a] *Center for Nanophase Materials Sciences, Oak Ridge National Laboratory, Oak Ridge, TN 37831, USA. E-mail: chim@ornl.gov*
[b] *Neutron Scattering Division, Oak Ridge National Laboratory, Oak Ridge, TN 37831, USA. E-mail: jalarvonh@ornl.gov, chengy@ornl.gov*
[c] *Department of Materials Science and Engineering, Massachusetts Institute of Technology, Cambridge, MA, 02139, USA*
[d] *School of Chemistry and Materials Science, University of Science and Technology of China (USTC), Hefei, Anhui 230026, China*
[e] *Mechanical Engineering, University of Michigan, Ann Arbor, MI 48109, USA*
[f] *Mechanical Engineering, Conn Center for Renewable Energy Research, University of Louisville, Louisville, KY, 40292, USA*
[g] *Department of Materials Science and Engineering, University of Michigan, Ann Arbor, MI 48109, USA*
[h] *JCNS-1, Forschungszentrum Jülich, D-52425 Jülich, Germany*

‡ Electronic supplementary information (ESI) available: Experimental details, simulation methods, TGA analysis, X-ray diffraction, calculated ratio of the scattering probability of LLZO and H-LLZO, refined structural parameters for protonated LLZO neutron diffraction, and lattice changes of H-LLZO as a function of proton concentration from DFT calculations. See DOI: 10.1039/c8ee02981d

§ These authors have contributed equally.

Aqueous Li-metal batteries are promising candidates for these and other emerging applications. Lithium metal as the anode holds the lowest reduction potential (−3.04 V) of any metal at ambient conditions and provides a high theoretical capacity (3860 mA h g^{-1}). In addition, aqueous catholytes have been reported to possess higher ionic conductivities and can be fabricated at lower costs compared to non-aqueous organic catholytes.[11,12] Nevertheless, Li metal is generally not compatible with aqueous electrolytes.[8,13–16] One approach to enable the integration of Li metal anodes with ALB is to interpose a solid-state electrolyte separator. The separator would prevent the reaction between Li and the aqueous electrolyte while potentially eliminating proton (H^+) cross-over and suppressing the reduction of protons to hydrogen gas at the Li anode. Ceramic electrolytes have been considered as a candidate for this application.[17–19]

Recent investigations on the garnet-type cubic LLZO, that is with the $Ia\bar{3}d$ symmetry, reveals that it has both high ionic conductivity ($\geq 10^{-4}$ S cm^{-1})[20–22] and good compatibility with Li metal. The LLZO–Li interface forms a thin self-limiting tetragonal-like LLZO interfacial layer that can effectively passivate the interface while maintaining reasonable ion conductivity that is expected to be $\sim 10^{-5}$ S cm^{-1} based on previous reports.[20,23–26] The crystal structure of the cubic polymorph (c-LLZO) was also found to be stable inside deionized water and in a wide range of pH without a significant drop in the ionic conductivity.[25] While it is recently revealed that when LLZO is immersed in water, it undergoes spontaneous Li^+/H^+ exchange, forming $(Li_{6.25-x}H_xAl_{0.25})La_3Zr_2O_{12}$ (H_x-LLZO),[25] yet it was unknown if both ions are mobile and whether protonated LLZO remains stable with lithium metal.[25,27–31] In this regard, demonstrating low mobility of H^+ in H_x-LLZO is crucial as the migration of H^+ towards the anode along with Li^+ during electrochemical cycling may cause undesired side reactions like $2H^+ \rightarrow H_2$, resulting in technological and safety issues. Even if this reaction does not occur, the migration of H^+ may lead to a non-unity transference number resulting in a concentration polarization at electrode interfaces, deteriorating the overall battery performance. Previous studies of protonated solid electrolytes are mainly focused on assessing the Li^+ distribution and structural stability in the tetragonal LLZO or other garnet-type solid electrolytes.[27–29,32,33] The individual ionic conduction behaviors of Li^+ or H^+ in c-LLZO at ambient temperature, however, have seldom been reported experimentally.[34] Without knowing the mobility of H^+ in cubic H_x-LLZO, one cannot conclusively argue that cubic LLZO is an appropriate separator for aqueous Li batteries.

Elucidating the mobility of H^+ and Li^+ ions individually in H_x-LLZO is challenging for traditional characterization methods. For instance, electrochemical impedance spectroscopy (EIS) has been widely used to evaluate ionic conductivity in materials. However, it is extremely challenging to configure right counter electrodes to differentiate ion diffusivity of H^+ and Li^+ when they coexist in a material. Structural characterization methods such as X-ray and electron diffractions are not sensitive to light elements and are unable to trace the mobility of H^+ and Li^+. In this study, by taking advantage of the significantly different neutron cross-sectional values of H^+ and Li^+ ions (H has 80 times higher signal than Li), we successfully differentiate the diffusion behavior of these two ions in H_x-LLZO using quasi-elastic incoherent neutron scattering (QENS).[35] A quantitative understanding of the ion diffusion kinetics in the H_x-LLZO was achieved by correlating the mean-square distributions from QENS with the ion occupancies and structural evolutions determined by neutron diffraction and electron spectroscopy. Our results show that while a moderate amount of ion exchange (~60% or lower) does not change the crystal structure, $Ia\bar{3}d$, of LLZO, an intensive exchange of H^+ ions (~75% or higher) introduces a slight distortion in the lattice, resulting in a phase transformation from $Ia\bar{3}d$ to $I\bar{4}3d$. Very importantly, we demonstrate that even with a significant extent of ion exchange, H^+ ions are almost immobile in cubic H_x-LLZO lattice at temperatures below 200 °C while a desirable Li^+ conductivity remains. These results confirm that LLZO can potentially be used as a protection layer for metallic lithium anode in aqueous Li batteries.

STEM and EELS were utilized to reveal the structural and chemical information of pristine LLZO and H_x-LLZO. A clear garnet structure was observed in pristine LLZO as noted by the high-angle annular dark-field (HAADF-STEM) and bright field (BF-STEM) images (Fig. 1a and b), which were recorded along the [001] zone axis. A corresponding $Ia\bar{3}d$ schematic model of garnet LLZO is shown as an overlay. After spontaneous Li^+/H^+ exchange, the garnet framework appears retained as seen in Fig. 1d and e. High-resolution TEM images of LLZO (Fig. 1c) and H_x-LLZO (Fig. 1f) clearly show the *d*-spacing along the (010) direction. Based on the length measurements in the corresponding intensity profiles, pristine LLZO has a cell parameter of a = 12.97 (±0.003) Å which agrees well with previous reports,[25,36] while protonated LLZO presents a slightly larger cell parameter of a = 13.07 (±0.005) Å. This change of the cell parameter is associated with the Li^+/H^+ exchange in the LLZO lattice. Quantitatively, the loss of Li content is estimated to be 70 (±2)% of the total Li in pristine LLZO, as calculated *via* the EELS analysis (Fig. 1g). Therefore, deep exchange of the Li^+ by H^+ results in an estimated composition of $(Li_{1.9}H_{4.4}Al_{0.25})La_3Zr_2O_{12}$. In comparison, our previous report shows that the ion exchange rate is ~60% after the c-LLZO is immersed in deionized water.[25] A higher ion exchange rate in this work should be attributed to the use of HNO_3 acid solution. Obvious changes in the fine structure of O *K*-edge was observed in Fig. 1h. In the O *K* doublet peaks, which are clearly present in the spectrum of pristine LLZO, exhibits different intensity ratio in H_x-LLZO: the first peak is replaced by a shoulder. This indicates the changes in the chemical bonding of O ions, further proving the ion exchange between Li^+ and H^+ in the LLZO structure.

In order to precisely determine the lattice structural changes in such intensive protonated LLZO, neutron diffraction paired with Rietveld refinement was performed. The $I\bar{4}3d$ structure well fits the pattern of the protonated LLZO (Fig. 2a) while the $Ia\bar{3}d$ model does not (additional fitting results are shown in ESI‡). A slight lattice structure modification was thus revealed, which is induced *via* a structural symmetry change from $Ia\bar{3}d$ (pristine) to $I\bar{4}3d$ (protonated). It is noted that such a slight structural change is not directly visualized *via* obvious characteristic peaks in the diffraction patterns. The Rietveld refinement along the entire

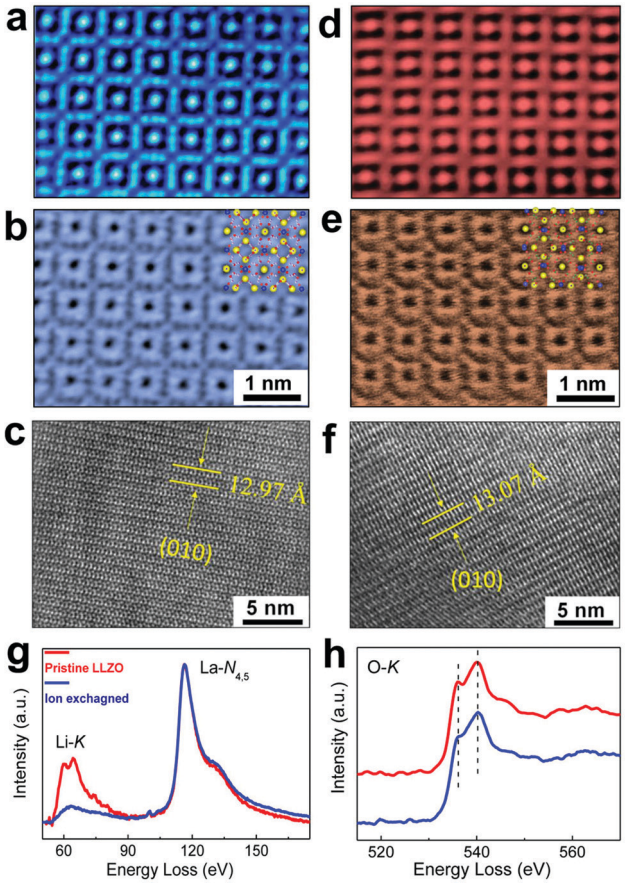

Fig. 1 HAADF-STEM (a), BF-STEM (b), and HRTEM (c) images of pristine LLZO. The overlay in (b) is the schematic model with $Ia\bar{3}d$ symmetry with a lattice parameter of 12.97 (±0.003) Å. HAADF-STEM (d), BF-STEM (e), and HRTEM (f) of H_x-LLZO. The schematic structure in (e) is with $I\bar{4}3d$ symmetry and a lattice parameter of 13.07 (±0.005) Å. *d*-Spacing was measured along (010) direction. The lattice parameter is averaged over 10 unit cells for high accuracy. All the images are recorded along [001] zone axis. Li-*K* (g) and O-*K* (h) EELS analyses of LLZO and H_x-LLZO.

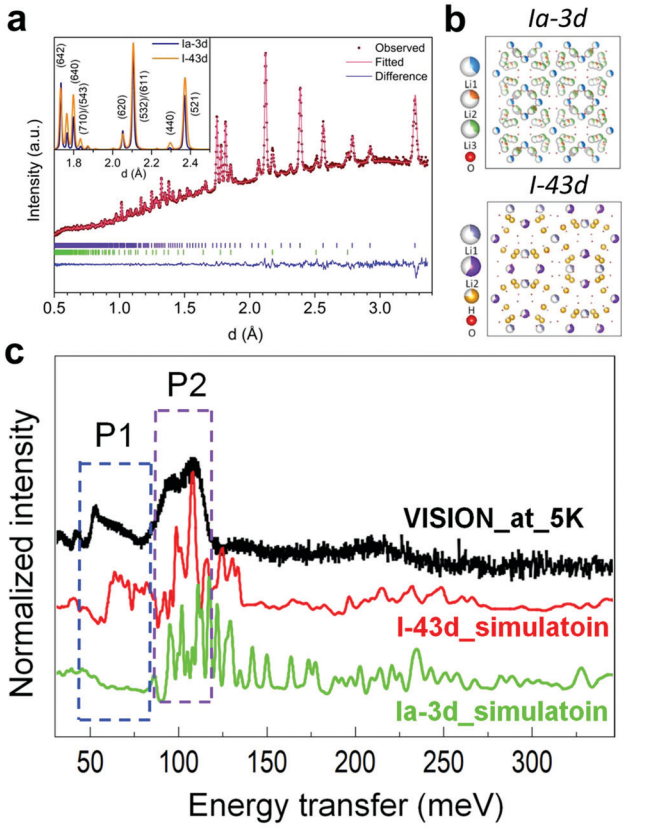

Fig. 2 (a) Neutron diffraction of protonated LLZO powders. The dots are the experimental data, while the red line through them is the calculated model. The series of tick marks on the top represents the H_x-LLZO, and the tick marks on the bottom indicate coexisting LiOH (7.6 ± 2.0 wt%). The bottom curves show the difference between the experimental data and calculated patterns. The inset shows the comparison of the fitted diffraction patterns of LLZO ($Ia\bar{3}d$) and H_x-LLZO($I\bar{4}3d$). Data extracted from this fit are given in Table S1 (ESI‡). (b) Schematic configurations of $Ia\bar{3}d$ and $I\bar{4}3d$ of H_x-LLZO. (c) Comparison between the experimental and calculated VISION-INS (inelastic neutron spectra) of H_x-LLZO with $I\bar{4}3d$ or $Ia\bar{3}d$ structure. P1 and P2 are the marked peaks that show an obvious difference between $I\bar{4}3d$ and $Ia\bar{3}d$ structure.

neutron diffraction pattern, which is sensitive to light elements, is a suitable approach to unravel the atomic rearrangement of Li and H in the lattice *via* capturing the peak intensity changes (Fig. 2a inset). The refined parameters of the protonated LLZO structure are listed in Table S1 (ESI‡). Additionally, a small amount of residual LiOH was also revealed. Per refinement, the lattice parameter of $I\bar{4}3d$ H_x-LLZO is 13.0704(2) Å, which is slightly larger than that of the $Ia\bar{3}d$ structure of pristine LLZO (12.98490(9) Å by neutron diffraction in the previous report),[34] agreeing with structural analysis by electron microscopy. Such a lattice expansion should be associated with the replacement of strong Li–O bonds by weaker hydrogen O–H···O bonds,[33] as suggested by density functional theory (DFT) calculations (see ESI‡).

The structural change in H_x-LLZO was further supported by inelastic neutron scattering (INS). Fig. 2c shows the INS spectrum of H_x-LLZO compared with the simulated reference spectra of the $Ia\bar{3}d$ and $I\bar{4}3d$ structures. The primary peaks in the experimental spectrum of H_x-LLZO, *i.e.* the peaks in the region ~50 meV and ~100 meV that are denoted as P1 and P2, match well with the simulated spectrum of $I\bar{4}3d$ simulation. The two structure models are shown in Fig. 2b. In addition to the determination of the $I\bar{4}3d$ structure, INS results prove that it is primary H^+ instead of H_3O^+ present in the H-LLZO structure. If there were significant H_3O^+ exchange, P1 is expected to be much stronger relative to P2, because the vibrational modes of the additional H_2O produce large H displacement and contribute to an intense vibrational band in the energy range of P1. The site occupancies of ions were further analyzed by neutron Rietveld refinement based on the NPD, as shown in Table S1 (ESI‡). In the protonated $I\bar{4}3d$ H_x-LLZO, the Li that typically resides in the tetrahedral 24d sites in cubic LLZO occupies the split tetrahedral 12a and 12b sites. The Li site occupancy is not equally distributed over these two sites, instead, for 0.34(6) and 0.63(7), respectively. Such Li occupancy is different from that of the protonated tetragonal LLZO, which is 0.340 and 0.908 for the 12a and 12b sites correspondingly, though the same crystal symmetry was reported.[27] Protons were found to

preferentially occupy the 48e crystallographic site with occupancy of 0.78(3). Such site occupancies result in a stoichiometry of $Li_{1.46(14)}H_{4.68(18)}Al_{0.25}La_3Zr_2O_{12}$ (with 75(±1)% total Li exchanged), agreeing well with the estimated Li content using EELS (~70% total Li exchange). In the rest of this manuscript, in order to be easily referred, we use the averaged exchange value of the quantifications from EELS and neutron diffraction, *i.e.* $Li_{1.7}H_{4.5}Al_{0.25}La_3Zr_2O_{12}$ ($H_{4.5}$-LLZO). It should be noted that this structure holds a good amount of vacancies that allows Li ions to hop, *i.e.* nominally 66 ± 7% at 12a, 37 ± 4% at 12b tetrahedral sites, and 22 ± 2% at the H-48e sites. These vacancies most likely allow the formation of a desirable percolation pathway for Li^+ ions to transport. As a result, protonated $H_{4.5}$-LLZO is expected to hold a reasonable Li^+ transport rate in the bulk.

The mobility of H^+ could significantly influence the stability of LLZO being used as a separator in aqueous Li batteries which primarily operate at RT. Precisely identifying hydrogen mobility is critical. Here, neutron scattering measurements were performed to probe H^+ and Li^+ diffusion dynamics. An overview of the temperature dependent dynamics in $H_{4.5}$-LLZO and pristine LLZO can be obtained by examining the elastic incoherent signal of BASIS spectra as a function of temperature (from 30 K to 500 K). An estimation of the average mean-square displacement (MSD) approximated from ion vibrations can be derived from the elastic integrated data, using Gaussian approximation.[37] As protons have a much larger neutron scattering cross-section (~80×) than that of Li, the MSD measured in $H_{4.5}$-LLZO is primarily attributed to proton diffusion and the contribution of Li^+ ions is negligible. The MSD derived from pristine LLZO, however, is primarily originated from Li^+ ion vibrations. As shown in Fig. 3, the temperature dependences of the MSD in the two samples are distinct. The neutron scattering measurements reflect the incoherent dynamics in the system instead of collective dynamics or structural information that can be obtained from coherent neutron scattering. Furthermore, Li dominates the incoherent signal (~56%), and the remaining signal arises mainly from La which is not expected to undergo diffusive motions at the chosen temperatures. Li^+ vibration in pristine LLZO shows clear Arrhenius temperature dependence throughout the entire temperature range. In $H_{4.5}$-LLZO, however, the MSD, which is dominated by the vibration of H^+ ions, remains nearly zero below 300 K and increases at a very slow rate at temperatures above 300 K. These results indicate that the Li^+ ions are mobile in pristine LLZO. The H^+ ions in $H_{4.5}$-LLZO, however, exhibit much fewer vibrations at low temperatures. Such a low vibration may indicate a low diffusivity of H^+ ions at RT as ion hopping in solids is associated with its lattice vibrations.[9,38] Even though there is controversy with regards to the proton mobility in Li garnets from previous investigations,[39] our results have unambiguous clarified the immobile nature of H^+ in cubic $(Li_{6.25-x}H_xAl_{0.25})La_3Zr_2O_{12}$. It should be mentioned that site occupancy and locations of Li^+ and H^+ in different garnets could potentially determine the ability of the lattice framework to trap H^+. In principle, the presence of proton ions in the lattice should meet two criteria for a solid electrolyte material used in aqueous Li batteries: low proton mobility and a minimum blockage to Li^+ ion mobility. The first criterion is associated with reducing the possible occurrence of hydrogen reduction reactions and preventing cross-over during cycling. While the second one is to ensure a sufficient lithium ion transport between lithium metal anode and aqueous solution.

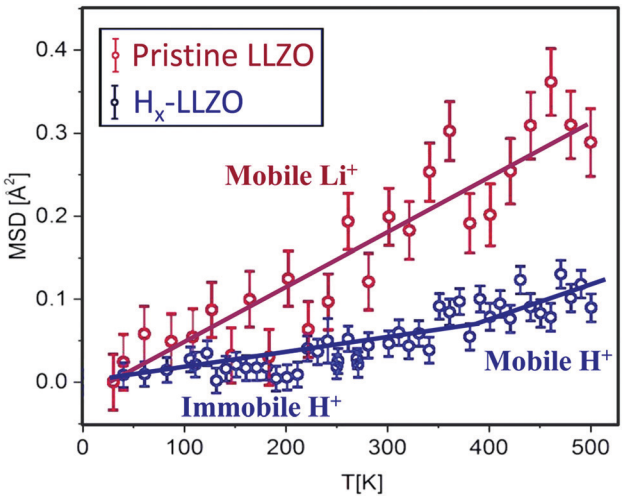

Fig. 3 The average mean-square-displacement for LLZO and H_x-LLZO samples. H has a larger neutron cross-section which yields a 90% of signal when coexists with Li. Li dominates the incoherent neutron scattering signal of pristine–LLZO and furthermore, the other elements in the sample are not expected to undergo diffusive motions in the measured temperatures, thus the MSD in pristine–LLZO reflects Li dynamics. In contrast, the MSD of H_x-LLZO is mainly a reflection of H.

QENS measures the dynamic structure factor, $S(Q,\omega)$, at a small energy transfer, ω, and at momentum transfers, Q, typically less than a few $Å^{-1}$. The measured $S(Q,\omega)$ is the Fourier transform in space and time of the self-correlation function. It provides information about the self-diffusive motions and can be used to derive diffusivity of ions. Fig. 4a and b present the experimentally observed HWHM *vs.* Q^2 fitted to Fick's law (HWHM = DQ^2 + c,

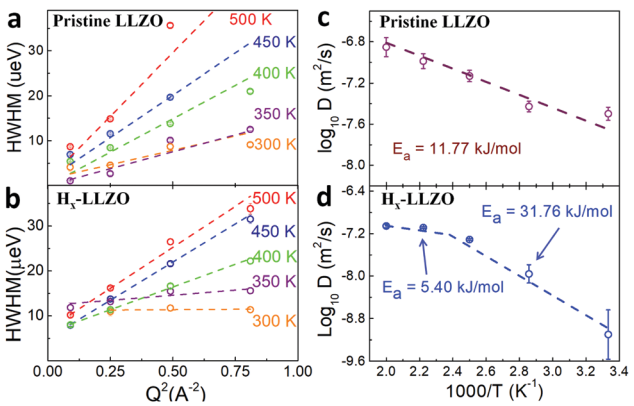

Fig. 4 Variation of HWHM with Q^2 for different temperatures of LLZO (a) and H_x-LLZO (b). The dashed lines represent fits of HWHM = DQ^2 + c, where D is the diffusion coefficient. Temperature dependence of the diffusion coefficient for (c) LLZO and (d) H_x-LLZO, respectively. There are two segments of the plot for H_x-LLZO that indicates a different diffusion mechanism at a higher temperature. Some of the error bars are smaller than the symbols.

where D is the diffusion coefficient and c is a constant) with the slope representing the diffusion coefficient.[40] While the fitted line for pristine LLZO approaches the origin, it was apparent that the fitted line does not approach the origin for $H_{4.5}$-LLZO. This result indicates that the diffusion is spatially constrained in $H_{4.5}$-LLZO. The limited extent of diffusion is especially evident in the lower temperature region, *i.e.* between 300 and 350 K (27 and 77 °C), where the HWHM values of the quasielastic components are nearly independent of Q. As established by MSD analysis and by comparing the elastic *vs.* QE intensities of the fitted QENS spectra, H^+ contributes mainly to the elastic part of the spectra, especially at the temperatures below 400 K. The MSD for $H_{4.5}$-LLZO up to 400 K follows Debye–Waller type of behavior, thus it is not expected that the H^+ contributes to the QE spectra. However, there is a change in the MSD slope around 400 K, after which the MSD increases more, indicating that H^+ begins to contribute to the QE part of the spectra. Thus H^+ is largely immobile in the measured timescale from 1 ps to 1 ns. Therefore, the diffusion coefficient reflects the Li^+ mobility in both of these two samples, except at temperatures above 400 K where H^+ partially contributes to the QE signal.

Based on the quasielastic scattering data, we further plot the diffusion coefficients of mobile ions in pristine LLZO and $H_{4.5}$-LLZO as a function of temperature, as shown in Fig. 4c and d. As expected, ionic diffusion in LLZO exhibits a single trend. In contrast, two dissimilar temperature dependences are observed in $H_{4.5}$-LLZO, suggesting the presence of distinct diffusion mechanisms within the low and high-temperature regions, respectively. In the low-temperature region (below 400 K), the H^+ is immobile and the diffusion coefficient is primarily attributed by Li^+ ions. At the higher temperature region (above 400 K), several potential possibilities could be involved in the conduction: (1) H^+ ions become mobile and change the overall diffusion mechanism in LLZO; (2) Li^+ ions take different diffusion pathways; or (3) Li^+ ions at certain lattice sites that are immobile become active at a high temperature.

The activation energy E_a for ion diffusion can be derived by fitting the Arrhenius law to the temperature dependence of the diffusion coefficients. Pristine LLZO exhibits linear behavior with the E_a of 11.77(±0.07) kJ mol^{-1} (Fig. 4c), which is slightly lower than previously reported values of hot-pressed LLZO pallets, which is ~26.00 kJ mol^{-1}.[20,41] A low activation energy could result from the use of nanoparticles, where a much higher surface area is present compared to that of polycrystalline bulk pellets in previous reports. It is known that ions often diffuse faster along surfaces compared to that of bulk, due to the presence of a large number of vacancies and uncoordinated chemical bonds. The activation energy of Li^+ ions in $H_{4.5}$-LLZO was estimated to be 31.76(±0.28) kJ mol^{-1} in the low-temperature regime (Fig. 4d), which is ~2.6× than that of pristine LLZO, indicating reduced Li^+ ion mobility in $H_{4.5}$-LLZO. It is noted that the derived diffusion coefficient at 300 K shows a relatively large error bar, which originates from the decreased ionic diffusion, thus lowering the sensitivity of our measurement. Such an error bar may affect the accuracy in the line fitting in Fig. 4d and result in an error in the estimation of activation energy in the low-temperature region. However, the transition temperature revealed in Fig. 4d matches well with that revealed in Fig. 3 for H_x-LLZO, indicating a valid/reasonable line fitting. The higher activation energy of Li^+ at the low T regime likely results from the presence of immobile H^+ ions in the lattice, which possibly impact the Li^+ migration pathway; or from the changes in Li^+ conduction channels in the lattice due to the lattice symmetry transformation.[27] Above 400 K, the activation energy is lowered to 5.40(±0.27) kJ mol^{-1}, which is possibly due to the activation of H^+ ions at high temperatures. It is noted that a weight loss was observed around 200 °C according to TGA results shown in Fig. S2 (ESI‡). Protons within the lattice of garnets somehow are expected to evolve out at high temperature and result in a change of diffusivity.[30,31] A potential structural or phase change at a high temperature also cannot be excluded.

This work provides new insights toward the development of LLZO for the use as an effective separator to protect Li-metal anodes used in advanced aqueous Li batteries. The primary criteria of a desirable protection layer include (i) structural and chemical stability in aqueous electrolyte, (ii) chemical and electrochemical compatibility with metallic lithium, (iii) high (~1 mS cm^{-1}) ionic conductivity, and (iv) stability over a relatively wide pH range to accommodate the change in the solution pH during cycling.[17,18,25] Our previous work shows that c-LLZO, after being immersed in de-ionized water, experiences spontaneous H^+ and Li^+ ion exchange up to 63.6%. The $Ia\bar{3}d$ structure is maintained in both neutral and base solution.[25] In the $Ia\bar{3}d$ structure, H^+ ions preferentially replace the Li^+ ions at the distorted octahedral sites, *i.e.* 96h. In this study, we focused on characterizing the stability of H_x-LLZO in acidic solution, and more importantly, on elucidating the mobility of H^+ and Li^+ ions. The immersion of c-LLZO in 0.01 M HNO_3 results in a higher ion exchange of Li^+ with H^+ (~75%), where not only the Li^+ ions at the 96h sites but also those at the 48g octahedral sites, are replaced by H^+. Despite such a high degree ion exchange, the cubic framework is well preserved with a slight structural distortion, resulting in a lattice symmetry transformation from to $Ia\bar{3}d$ to $I\bar{4}3d$. Fig. 5 briefly clarifies the difference of the lattice structure and ion occupancies between pristine LLZO and H_x-LLZO at the unit cell level.

By taking advantage of the dramatic difference in neutron cross-section for H^+ and Li^+ ions, we unambiguously revealed that H^+ is immobile at temperatures below 400 K in protonated LLZO, regardless of a high concentration in the structure (75% exchange). The immobility of H^+ ions in the lattice is beneficial

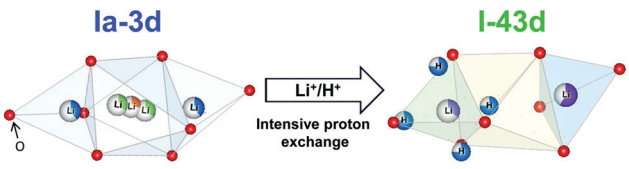

Fig. 5 Schematic illustrations of structural and chemical modifications in c-LLZO after intensive proton exchange; the structure and ion occupancies of pristine $Ia\bar{3}d$ LLZO are delineated based on previous reports.[42,43] Those for $I\bar{4}3d$ LLZO are shown based on current work, *e.g.* Fig. 2 and Table S1 (ESI‡).

for the application of LLZO in aqueous batteries. Such immobility prevents migration of the H^+ ions to the LLZO/Li interface and reacting with Li metal. Given the fact that the working temperature of practical aqueous rechargeable lithium batteries is typically far below this temperature, the reduction reaction of H^+ with Li metal should be prevented. In contrast to H^+ ions, Li^+ ions have a reasonable ionic conductivity in the $H_{4.5}$-LLZO. This property is based on the combined information from elastic and quasi-elastic neutron scattering. As revealed by MSD, H^+ ions are immobile below 400 K in $H_{4.5}$-LLZO. Li^+ ions, however, are mobile since pristine c-LLZO shows a distinct MSD slope compared to that of $H_{4.5}$-LLZO. The diffusion-related phenomena observed in $H_{4.5}$-LLZO at low temperatures, therefore, should be primarily contributed by Li^+ ions. Therefore, the activation energy of Li^+ ions can be estimated from diffusion coefficients measured using quasi-elastic scattering data. A higher activation energy of Li^+ ions was observed in protonated LLZO compared to that in pristine LLZO, which should arise from the presence of immobile H^+ in the lattice. The presence of H^+ could influence the Li^+ ion conduction primarily in three ways: first, the H^+ replace Li^+ ions, largely reducing the concentration of Li^+ in the structure; second, the H^+ ions are immobile and may block the normal Li^+ ion percolation pathway in the structure; third, the replacement of Li^+ with H^+ ions in the lattice could induce lattice structure distortions therefore possibly altering the bottleneck size of Li^+ ion migration. This effect can be clearly understood in the case of $H_{3.7}$-LLZO with a moderate degree of H^+ exchange where the $Ia\bar{3}d$ structured is maintained.[44,45] In $Ia\bar{3}d$ structured H_x-LLZO, the Li^+ migration pathway involves the connection of both octahedral Li sites and face-sharing Li tetrahedral sites. A precise understanding of how the presence of a higher concentration of H^+ in $I\bar{4}3d$ structure influences Li^+ ion conduction requires detailed theoretical calculations. It is certain that the presence of H^+ in c-LLZO alters the transport behavior of Li^+. Given the high ionic conductivity of LLZO (10^{-4}–10^{-3} S cm^{-1} at room temperature) and an activation energy of 31.76 kJ mol^{-1} of $H_{4.5}$-LLZO, it must be pointed out that a reasonable Li^+ ion conductivity of $\sim 10^{-6}$–10^{-5} S cm^{-1} in $H_{4.5}$-LLZO is expected. As most of the current aqueous batteries do not operate at an elevated temperature, our results indicate that the H^+ ions do not diffuse to Li metal when LLZO is used as a separator layer in aqueous Li batteries with a neutral or slightly acidic environment.

Conclusion

This work elucidates the individual ion mobility of H^+ and Li^+ and the structural stability in $H_{4.5}$-LLZO for its application as a protection layer for Li metal in aqueous lithium batteries. It was found that even a relatively high Li^+/H^+ ion exchange (75%) in LLZO, that is induced by immersing LLZO in 0.01 M HNO_3 for 30 min, does not change the cubic framework. Instead, lattice distortion is induced, leading to a phase transformation from $Ia\bar{3}d$ to $I\bar{4}3d$. Most importantly, we undoubtedly probe the individual ion diffusion behavior of H^+ and Li^+ ions in $H_{4.5}$-LLZO, which is otherwise challenging to conventional characterization techniques. We found out that while Li^+ ions show good ion mobility in the structure, the H^+ ions are immobile at RT. Such inactivity of H^+ ions should contribute to the interfacial stability of LLZO being used as a protection layer for Li-metal in aqueous Li batteries. The activation energy of Li^+ is estimated to be around 31.76 kJ mol^{-1} at room temperature, indicating reasonable Li^+ ion conduction in $H_{4.5}$-LLZO. Our results, therefore, suggest that LLZO is a promising candidate to be used as a protection layer in aqueous lithium batteries. More importantly, our work provides a new method to probe diffusion behavior of different ions in solids that contain multiple mobile ion species, an important family of materials for energy storage, neuromorphic computing, environmental sensing, and beyond.

Author contributions

M. Chi and Y. Cheng conceived the study. X. Liu and M. Chi wrote the manuscript. X. Liu and C. Ma performed the TEM/EELS experiments; Y. Chen, K. An, Y. Cheng, and N. H. Jalarvo performed the experiments and analysed the results from Neutron scattering. Z. D. Hood, A. Sharafi, H. Wang and J. Sakamoto synthesized the materials; S. Yu and D. J. Siegel performed DFT calculations. All authors contributed to the discussion of the results and the manuscript editing.

Conflicts of interest

There are no conflicts to declare.

Acknowledgements

Research sponsored by the U.S. Department of Energy (DOE), Office of Science, Basic Energy Sciences, Materials Sciences and Engineering Division (X. L., M. C.). Research conducted at ORNL's Center for Nanophase Materials Sciences (CNMS) (C. M., M. C.) and the Spallation Neutron Source (SNS) (Y. C., K. A., N. H. J., Y. C.), both of which are U.S. DOE Office of Science User Facilities. H. W. thanks the support by the EVPRI Internal Grant and Conn Center for Renewable Energy Res. at U. Louisville. Z. D. H. acknowledges support from the NSF Graduate Research Fellowship (DGE-1650044). J. S., S. S., and D. S. thanks the support by the U.S. DOE, Office of Energy Efficiency and Renewable Energy (Award DE-EE00006821). S. Y. thanks support by the Kwanjeong Educational Foundation.

References

1 E. Quartarone and P. Mustarelli, *Chem. Soc. Rev.*, 2011, **40**, 2525.
2 D. Lin, Y. Liu and Y. Cui, *Nat. Nanotechnol.*, 2017, **12**, 194–206.
3 J. W. Choi and D. Aurbach, *Nat. Rev. Mater.*, 2016, **1**, 16013.
4 J. B. Goodenough and K.-S. Park, *J. Am. Chem. Soc.*, 2013, **135**, 1167–1176.
5 N. Nitta, F. Wu, J. T. Lee and G. Yushin, *Mater. Today*, 2015, **18**, 252–264.

6 W. Tang, Y. Zhu, Y. Hou, L. Liu, Y. Wu, K. P. Loh, H. Zhang and K. Zhu, *Energy Environ. Sci.*, 2013, **6**, 2093.
7 J. B. Goodenough, *Electrochem. Soc. Interface*, 2016, **25**, 67–70.
8 P. G. Bruce, S. A. Freunberger, L. J. Hardwick and J.-M. Tarascon, *Nat. Mater.*, 2011, **11**, 19–29.
9 J. C. Bachman, S. Muy, A. Grimaud, H.-H. Chang, N. Pour, S. F. Lux, O. Paschos, F. Maglia, S. Lupart, P. Lamp, L. Giordano and Y. Shao-Horn, *Chem. Rev.*, 2016, **116**, 140–162.
10 S. Chu, Y. Cui and N. Liu, *Nat. Mater.*, 2016, **16**, 16–22.
11 Y. Wang, J. Yi and Y. Xia, *Adv. Energy Mater.*, 2012, **2**, 830–840.
12 W. Xu, J. Wang, F. Ding, X. Chen, E. Nasybulin, Y. Zhang and J.-G. Zhang, *Energy Environ. Sci.*, 2014, **7**, 513.
13 N. Imanishi and O. Yamamoto, *Mater. Today*, 2014, **17**, 24–30.
14 P. He, T. Zhang, J. Jiang and H. Zhou, *J. Phys. Chem. Lett.*, 2016, **7**, 1267–1280.
15 S. Hasegawa, N. Imanishi, T. Zhang, J. Xie, A. Hirano, Y. Takeda and O. Yamamoto, *J. Power Sources*, 2009, **189**, 371–377.
16 H. Nemori, K. Rahman, H. Izumi, S. Mitsuoka, X. Shang, O. Yamamoto, N. Imanishi and M. Nomura, *Meet. Abstr.*, 2016, 842.
17 Y. Lu, J. B. Goodenough and Y. Kim, *J. Am. Chem. Soc.*, 2011, **133**, 5756–5759.
18 M. Balaish, A. Kraytsberg and Y. Ein-Eli, *Phys. Chem. Chem. Phys.*, 2014, **16**, 2801.
19 A. Manthiram and L. Li, *Adv. Energy Mater.*, 2015, **5**, 1401302.
20 R. Murugan, V. Thangadurai and W. Weppner, *Angew. Chem., Int. Ed.*, 2007, **46**, 7778–7781.
21 E. Rangasamy, J. Wolfenstine and J. Sakamoto, *Solid State Ionics*, 2012, **206**, 28–32.
22 R. Koerver, W. Zhang, L. de Biasi, S. Schweidler, A. O. Kondrakov, S. Kolling, T. Brezesinski, P. Hartmann, W. G. Zeier and J. Janek, *Energy Environ. Sci.*, 2018, **11**, 2142.
23 C. Ma and M. Chi, *Front. Energy Res.*, 2016, **4**, 23.
24 C. Ma, Y. Cheng, K. Yin, J. Luo, A. Sharafi, J. Sakamoto, J. Li, K. L. More, N. J. Dudney and M. Chi, *Nano Lett.*, 2016, **16**, 7030–7036.
25 C. Ma, E. Rangasamy, C. Liang, J. Sakamoto, K. L. More and M. Chi, *Angew. Chem.*, 2015, **127**, 131–135.
26 J. L. Allen, J. Wolfenstine, E. Rangasamy and J. Sakamoto, *J. Power Sources*, 2012, **206**, 315–319.
27 A. Orera, G. Larraz, J. A. Rodríguez-Velamazán, J. Campo and M. L. Sanjuán, *Inorg. Chem.*, 2016, **55**, 1324–1332.
28 G. Larraz, A. Orera, J. Sanz, I. Sobrados, V. Diez-Gómez and M. L. Sanjuán, *J. Mater. Chem. A*, 2015, **3**, 5683–5691.
29 G. Larraz, A. Orera and M. L. Sanjuán, *J. Mater. Chem. A*, 2013, **1**, 11419.
30 C. Galven, J.-L. Fourquet, M.-P. Crosnier-Lopez and F. L. Berre, *Chem. Mater.*, 2011, **23**, 1892–1900.
31 L. Truong and V. Thangadurai, *Inorg. Chem.*, 2012, **51**, 1222–1224.
32 L. Truong, M. Howard, O. Clemens, K. S. Knight, P. R. Slater and V. Thangadurai, *J. Mater. Chem. A*, 2013, **1**, 13469.
33 C. Galven, J. Dittmer, E. Suard, F. Le Berre and M.-P. Crosnier-Lopez, *Chem. Mater.*, 2012, **24**, 3335–3345.
34 Z. F. Yow, Y. L. Oh, W. Gu, R. P. Rao and S. Adams, *Solid State Ionics*, 2016, **292**, 122–129.
35 E. Mamontov and K. W. Herwig, *Rev. Sci. Instrum.*, 2011, **82**, 085109.
36 Y. Chen, E. Rangasamy, C. R. dela Cruz, C. Liang and K. An, *J. Mater. Chem. A*, 2015, **3**, 22868–22876.
37 N. Jalarvo, M. Tyagi and M. K. Crawford, *EPJ Web Conf.*, 2015, **83**, 02007.
38 K. Wakamura, *Phys. Rev. B: Condens. Matter Mater. Phys.*, 1997, **56**, 11593–11599.
39 M. L. Sanjuán, A. Orera, I. Sobrados, A. F. Fuentes and J. Sanz, *J. Mater. Chem. A*, 2018, **6**, 2708–2720.
40 M. J. Klenk, S. E. Boeberitz, J. Dai, N. H. Jalarvo, V. K. Peterson and W. Lai, *Solid State Ionics*, 2017, **312**, 1–7.
41 V. Thangadurai, D. Pinzaru, S. Narayanan and A. K. Baral, *J. Phys. Chem. Lett.*, 2015, **6**, 292–299.
42 Y. Li, J.-T. Han, C.-A. Wang, S. C. Vogel, H. Xie, M. Xu and J. B. Goodenough, *J. Power Sources*, 2012, **209**, 278–281.
43 Y. Chen, E. Rangasamy, C. Liang and K. An, *Chem. Mater.*, 2015, **27**, 5491–5494.
44 K. Meier, T. Laino and A. Curioni, *J. Phys. Chem. C*, 2014, **118**, 6668–6679.
45 X. He, Y. Zhu and Y. Mo, *Nat. Commun.*, 2017, **8**, 15893.